

## Spin-Polarized Fractional Corner Charges and Their Photonic Realization

Ran Gladstein Gladstone<sup>1,\*</sup>, Minwoo Jung,<sup>2</sup> and Gennady Shvets<sup>1</sup>

<sup>1</sup>*School of Applied and Engineering Physics, Cornell University, Ithaca, New York 14853, USA*

<sup>2</sup>*Department of Physics, Cornell University, Ithaca, New York 14853, USA*

 (Received 13 June 2021; accepted 15 December 2021; published 10 January 2022)

We demonstrate that a spin degree of freedom can introduce additional texture to higher order topological insulators (HOTIs), manifesting in novel topological invariants and phase transitions. Spin-polarized mid-gap corner states of various multiplicities are predicted for different HOTI phases, and novel bulk-boundary correspondence principles are defined based on bulk invariants such as total and spin corner charge. Those are shown to be robust to spin-flipping perturbations. Photonic realizations of spin-linked topological phases are demonstrated in engineered systems using pseudospin.

DOI: 10.1103/PhysRevLett.128.026801

The interplay between spin and topology has long been of interest to physicists [1–5]. Shortly after the prediction of time-reversal (TR) preserving Chern insulators [6], the concept was extended to spinful electrons, leading to the prediction [7] and experimental realization of the quantum spin Hall (QSH) effect [8,9]. The extension to spinful systems typically involves doubling of the Hilbert space to include two similar copies of the original spinless system [7,10], and can have significant effect on the topology of the system. While the Chern insulator has a  $\mathbb{Z}$  topological invariant, a spin Chern insulator possesses a  $\mathbb{Z}_2$  topological invariant due to TR and inversion symmetries [11]. The addition of spin to the system has, therefore, changed its topological classification.

More recently, these concepts have been extended to higher order topological insulators (HOTIs) [12–19], and their photonic and phononic counterparts (PHOTIs) [20–28]. A HOTI is a  $d$ -dimensional topological insulator with a bulk topological invariant predicting topological states localized on some of its  $d - n$  dimensional terminations, where  $n \in \mathbb{N}$  and  $2 \leq n \leq d$ . HOTIs can support fractional boundary charges due to a combination of their bulk modes, edge modes, hinge modes, etc. Wannier centers being localized at the edges of the unit cell, contributing a fractional number of electronic charge [12]. This fractional charge is related to the mode density at the boundaries of the HOTI and can be measured with regard to the mode density at the terminations of the bulk [14]. It is natural to ask if spinful HOTIs have any emerging topological properties and classification that distinguish them from their spinless counterparts. Most of the research of spinful HOTIs has so far concentrated on the systems with fermionic TR symmetry [16,17] or time-dependent drive [15].

In this Letter we examine the effects of adding the spin degree of freedom (DOF) to HOTIs when fermionic TR symmetry is broken yet bosonic TR symmetry is maintained [10,29]. Our analysis also applies to pseudospin DOFs, such as layer [30–33] and polarization [34–36]. We

use the latter to emulate spinful PHOTIs based on engineered microwave structures. The specific 2D lattice models and their corresponding periodic electromagnetic waveguides considered in this Letter possess  $C_6$  symmetry, and are additionally endowed with Kekulé texture [21,37,38], spin DOF, and a symmetry-preserving spin-flipping perturbation coupling the spin- $\uparrow$  and spin- $\downarrow$  components. The latter will be assumed in the form of Kane-Mele spin-orbit coupling (SOC) [1]. For spinless lattice models, such topological crystalline insulators (TCIs) have been shown to support a HOTI phase with a quantized fractional corner charge of  $Q_c = 1/2$  [39].

Below we demonstrate that when an independent spin subspace is introduced, two nontrivial phases can emerge: a phase possessing two quantized spin-polarized fractional corner charges  $Q_c^{\uparrow,\downarrow} = 1/2$  (spin-HOTI), and a phase characterized by a single quantized fractional corner charge  $Q_c = 1/2$  (HOTI). While in the absence of SOC the spin-HOTI phase can be thought of as being independently topological for each of the spin states [24]; such simple interpretation is no longer valid in the presence of a finite spin-flipping SOC. Which one out of these two phases is realized depends on the strength of the SOC that couples the two spin states, and on the individual topological properties of each spin component in the absence of such coupling. We further demonstrate that the distinct properties of the spin-HOTI and HOTI phases manifest themselves in different multiplicities and spin textures of their corresponding zero-energy corner states.

Our starting point is the tight binding (TB) model on a honeycomb lattice schematically shown in Fig. 1(a):

$$H = \sum_{\langle ij \rangle} t_{\text{in}}^{\uparrow} c_{i\uparrow}^{\dagger} c_{j\uparrow} + \sum_{\langle i'j' \rangle} t_{\text{out}}^{\uparrow} c_{i'\uparrow}^{\dagger} c_{j'\uparrow} + \sum_{\langle ij \rangle} t_{\text{in}}^{\downarrow} c_{i\downarrow}^{\dagger} c_{j\downarrow} + \sum_{\langle i'j' \rangle} t_{\text{out}}^{\downarrow} c_{i'\downarrow}^{\dagger} c_{j'\downarrow} + \sum_{\langle\langle ij \rangle\rangle\alpha\beta} \frac{i}{3\sqrt{3}} \lambda_{\text{SOC}} \nu_{ij} s_{\alpha\beta}^x c_{i\alpha}^{\dagger} c_{j\beta}, \quad (1)$$

where  $c_{i\uparrow(\downarrow)}$  is the spin- $\uparrow$  ( $\downarrow$ ) electron creation operator at the  $i$ th lattice site,  $\nu_{ij}$  is  $+1$  for counter-clockwise direction next-nearest neighbor terms and  $-1$  for clockwise direction next-nearest neighbor terms,  $s_{\alpha\beta}^x$  are the matrix elements of the  $\hat{s}_x$  Pauli matrix, and  $\lambda_{\text{SOC}}$  is the strength of SOC coupling. The first (third) term describes the nearest neighbor intra unit cell hopping of the spin up (down) electrons, the second (fourth) term describes the nearest neighbor inter unit cell hopping of the spin- $\uparrow$  ( $\downarrow$ ) electrons, and the fifth term describes the next-nearest neighbor Kane-Mele SOC [1].

Numerous works in photonics and phononics have implemented the first two terms of Eq. (1) [21,26,40–42] but no implementation of the full Eq. (1) has been presented yet. While those platforms emulate a Kekulé lattice distortion (frequently labeled as orbital pseudospin), giving rise to edge and one-per-corner states, they do not implement a spinful Kekulé lattice distortion model—a serious limitation that prevents access to the novel spin-HOTI topological phase supporting two distinct localized state per corner as described below. Additional richness of the spinful model with SOC [Eq. (1)] that cannot be achieved with existing platforms enables phase transitions between the trivial, HOTI, spin-HOTI, and QSH phases.

Fourier transforming from the real space to the Bloch quasimomentum space [43] results in the reciprocal unit cell depicted in Fig. 1(b), where the high symmetry points (HSPs) [44] are  $\Gamma = (0, 0)$ ,  $K = (4\pi/3/a, 0)$ ,  $M = \pi/a(1, 1/\sqrt{3})$  and  $a$  is the real space lattice constant, i.e., the distance between neighboring unit cells. All band structures in this Letter are calculated along the reduced Brillouin Zone depicted with a dashed blue triangle. Without loss of generality, we assume that all hopping amplitudes are positive, and that the energy scale is defined by setting  $(t_{\text{out}}^{\uparrow,\downarrow} + t_{\text{in}}^{\uparrow,\downarrow})/2 = 1$ .

The difference between intercell and intracell hopping amplitudes,  $\Delta_{\uparrow,\downarrow} \equiv t_{\text{out}}^{\uparrow,\downarrow} - t_{\text{in}}^{\uparrow,\downarrow}$ , determines the topology of the two uncoupled spin subspaces in the absence of SOC: each spin component's subspace behaves independently as a HOTI for  $\Delta_{\uparrow,\downarrow} > 0$ , or a trivial insulator for  $\Delta_{\uparrow,\downarrow} < 0$ , as shown in Fig. 1(c). When both independent subspaces are in the HOTI topological phase simultaneously, we name the resulting phase spin-HOTI, which in this case is a somewhat redundant phase that can be viewed as two orthogonal HOTI copies. The topological phase transitions at  $\Delta_{\uparrow,\downarrow} = 0$  are the consequences of the band inversions between  $p$ - and  $d$ -orbital mode profiles [21,38]: the energies of the  $p$ -orbital bands are below (above) the band gap for trivial (topological) insulators.

The unperturbed spin corner charges  $\tilde{Q}_c^{\uparrow,\downarrow}$  are separately defined for each spin subspace [39]. Corner charges can be calculated based on the symmetry properties of the propagation bands below the band gap at the high-symmetry  $\Gamma$  and  $M$  points of the Brillouin zone [39]:

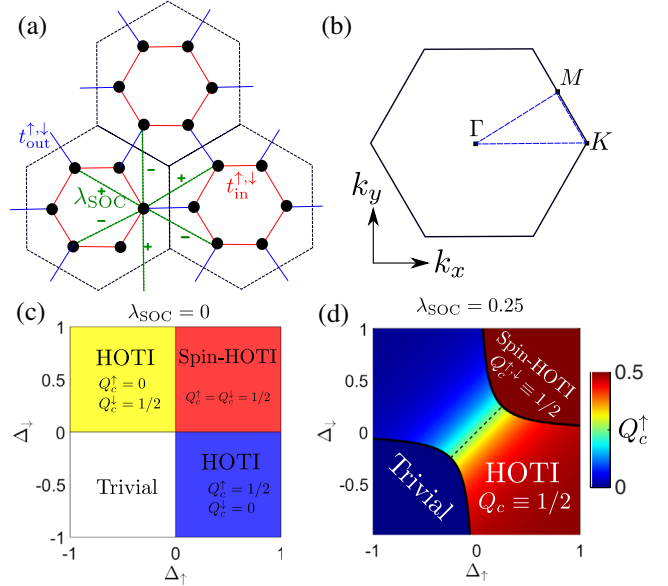


FIG. 1. Spinful HOTI: the tight-binding model and its phase diagrams. (a) Schematic of the TB model with definitions of intracell (red lines) and intercell (blue lines) hopping amplitudes. Black circles: lattice sites; dashed hexagons: unit cells; green dashed lines: spin-orbit coupling amplitudes  $\lambda_{\text{SOC}}$  and their signs ( $\pm$ ). (b) Brillouin zone (black hexagon), reduced Brillouin zone (dashed blue triangle), and high symmetry points of the reciprocal lattice. (c),(d) Phase diagram at constant  $\lambda_{\text{SOC}} = 0$  (c) and  $\lambda_{\text{SOC}} = 0.25$  (d). Solid curves: bulk band gap closure at  $\lambda_{\text{SOC}} = \lambda_{\text{SOC}}^{\text{th}}(\Delta_{\uparrow}, \Delta_{\downarrow})$ ; color bar:  $Q_c^{\uparrow}$  for trivial, spin-topological, and topological (not quantized) phases. Dashed line: spin-degeneracy  $\Delta_{\uparrow} = \Delta_{\downarrow}$  corresponding to quantum spin-Hall phase.

$$\tilde{Q}_c^{\uparrow,\downarrow} = (\#M_{\uparrow,\downarrow} - \#\Gamma_{\uparrow,\downarrow})/4 \quad (2)$$

where  $\#M_{\uparrow}$  ( $\#\Gamma_{\uparrow}$ ) is the number of  $C_2$ -invariant spin- $\uparrow$  modes below the band gap at the  $M$  ( $\Gamma$ ) point (same for spin- $\downarrow$  modes).

When the spin components are coupled through the SOC, the expressions for  $\tilde{Q}_c^{\uparrow,\downarrow}$  are no longer quantized, and must be redefined because of the mixing between the spin- $\uparrow$  and spin- $\downarrow$  contents of the propagation bands. Therefore, we modify the definitions of the corner charges by weighing the contribution of each band by its spin- $\uparrow/\downarrow$  content:

$$Q_c^{\uparrow,\downarrow} = \frac{1}{4} \sum_i (|\langle \uparrow, \downarrow | \psi_i(M) \rangle|^2 - |\langle \uparrow, \downarrow | \psi_i(\Gamma) \rangle|^2), \quad (3)$$

where  $|\psi_i(\mathbf{k})\rangle$  is the wave function of a  $C_2$ -invariant band  $i$  below the band gap at the  $\mathbf{k} = M, \Gamma$  points. Since spin is an intrinsic electron property Eq. (3) can be calculated even when the spin subspaces are mixed.

It can be shown that  $Q_c^{\uparrow,\downarrow}$  defined by Eq. (3) are quantized at  $Q_c^{\uparrow,\downarrow} = 1/2$  for the spin-HOTI, and at  $Q_c^{\uparrow,\downarrow} = 0$  for the trivial phase. Briefly, the probability conservation

for all the bands below the band gap ensures that  $Q_c^{\uparrow,\downarrow} = \tilde{Q}_c^{\uparrow,\downarrow}$  for these two cases. This is due to the lack of cross-band transitions generated by the  $C_6$  symmetry-preserving SOC: the  $d$  ( $p$ ) orbitals for both spins are on the same side of the band gap, and the SOC only connects the orbitals of one spin component to the same orbitals of the other component (see the Supplemental Material [45] for details). This conservation of probability is independent of choice of spin basis, and therefore Eq. (3) can be calculated using any spin basis with the result unchanged.

On the contrary,  $Q_c^{\uparrow,\downarrow}$  corner charges are not separately quantized in the HOTI phase. The cause of this transition from either trivial to HOTI (if  $\Delta_{\uparrow\downarrow} < 0$ ) phase, or from spin-HOTI to HOTI (if  $\Delta_{\uparrow\downarrow} > 0$ ) is the band inversion by the strong SOC coupling satisfying  $\lambda_{\text{SOC}} > \lambda_{\text{SOC}}^{(\text{th})}$ . Here  $\lambda_{\text{SOC}}^{(\text{th})} \equiv \sqrt{\Delta_{\uparrow}\Delta_{\downarrow}}$  is the threshold value of the SOC strength corresponding to the closing of the bulk band gap, and followed by band inversion. However, the total spin-independent corner charge  $Q_c = Q_c^{\uparrow} + Q_c^{\downarrow} = 1/2$  remains quantized in the HOTI phase, thus making it topologically nontrivial. Phase diagrams in the  $(\Delta_{\downarrow}, \Delta_{\uparrow})$  space showing one trivial and two topological (spin-HOTI and HOTI) phases are shown in Figs. 1(c) and 1(d) for constant  $\lambda_{\text{SOC}}$ . The spin-degeneracy region  $\Delta_{\uparrow} = \Delta_{\downarrow}$  represented by the dashed line in Fig. 1(d) corresponds to the fermionic TR symmetric QSH phase [38,46] embedded in a bosonic TR symmetric HOTI phase (see Supplemental Material [45]).

To investigate the existence and multiplicity of zero-energy corner states (ZCSs), we consider an interface between trivial and topological domains containing a single  $120^\circ$  corner, as shown in the upper-left inset in Fig. 2(a). In the case when the topological phase is a HOTI, its single quantized topological charge  $Q_c = 1/2$  manifests itself as a single spin-polarized ZCS. The spectrum for such corner-containing domain wall is calculated using a finite-domain TB calculation and is shown in Fig. 2(a) (see Table S1 [45] for the TB parameters). The existence of the ZCS is a direct consequence of the quantized bulk invariant  $Q_c$  and of the chiral symmetry present in a  $C_6$  lattice with Kekulé distortion, both of which are preserved even with finite SOC (see Supplemental Material [45]).

The existence of the separate quantized spin charges  $Q_c^{\uparrow} = Q_c^{\downarrow} = 1/2$  in the spin-HOTI phase guarantees a degenerate pair of ZCSs [see Fig. 2(b)] with distinct spin textures, as long as  $\Delta_{\uparrow,\downarrow} > 0$  and  $\lambda_{\text{SOC}} < \lambda_{\text{SOC}}^{(\text{th})}$ . This is in contrast to the spinless model [39] that only considers  $Q_c$  and thus predicts no ZCSs for the spin-HOTI phase. The localization lengths of the two corner states are generally not equal, and are determined by the hopping amplitudes,  $\lambda_{\text{SOC}}$ , as well as the size of the band gap between the edge states. The latter can be modified by the choice of hopping amplitudes along the domain wall [21].

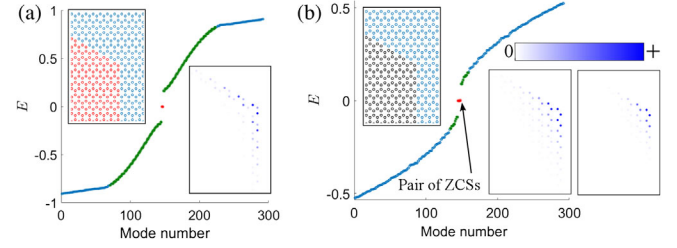


FIG. 2. Properties of corner-shaped domain walls between a topological [(a) HOTI and (b) spin-HOT] and a trivial phase: a TB model. A corner of a HOTI/trivial (spin-HOTI or trivial) interface supports one (two) ZCS. Upper-left inset in (a): domain wall shape. Energy spectra: bulk (blue), edge (green), and corner (red) modes for the HOTI or trivial (a) and spin-HOTI or trivial (b) interfaces. Lower-right inset in (a): intensity of the single ZCS. Upper-left inset in (b): domain wall shape. Lower-right insets in (b): intensities of the two ZCSs. TB model parameters: see Table S1 [45].

Next, we present a photonic platform that can be used for emulating a spinfull HOTI described by the Hamiltonian given by Eq. (1). The structure shown in Fig. 3(a) is comprised of a photonic crystal (PhC) waveguide made of perfect electric conductors (PEC) elements sandwiched between two PEC plates [34–36]: see the Supplemental

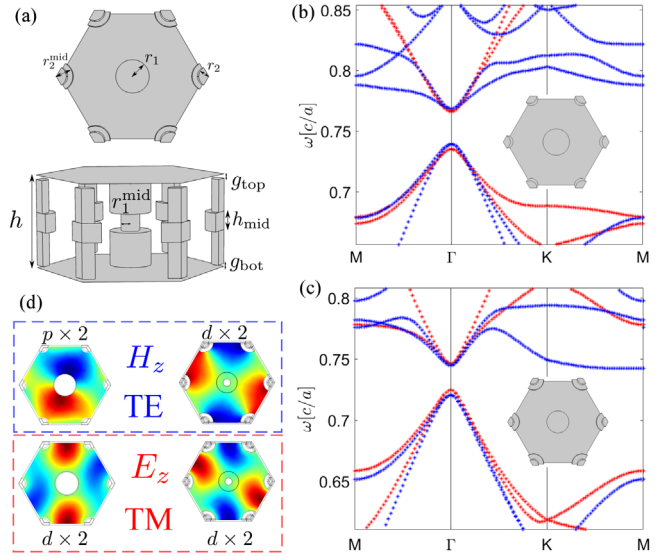


FIG. 3. Emulation of spinful PHOTIs using a photonic crystal waveguide with Kekulé distortion. (a) Top and side views of the PhC unit cell with intercell distance  $a$ . (b),(c) Band structures for PHOTI (b) and spin-PHOTI (c) designs. TE (blue symbols) and TM (red symbols) are degenerate at the  $\Gamma$  point. (d) Field profiles of four of the eight modes at  $z = h/2$  of the  $\mathbf{p}$  and  $\mathbf{d}$  orbital bands below the band gap at the  $\Gamma$  point for PHOTI (left column) and  $\mathbf{d}$  only spin-PHOTI (right column) for TE (dashed blue box) and TM (dashed red box) electromagnetic modes. The modes not shown, indicated by  $\times 2$ , are degenerate and identical to the ones shown up to  $120^\circ$  rotation. Parameters: symmetric air gaps  $g_{\text{top}} = g_{\text{bot}}$ ; see Table S2 [45] for details.



Material [45] for the geometric parameters of all PhC designs. The PhC possesses  $C_6$  symmetry, thereby allowing a Kekulé distortion [47]. In the case of symmetric air gaps ( $g_{\text{top}} = g_{\text{bot}}$ ) between the PhC elements and the plates, the mid-plane mirror symmetry  $z \rightarrow -z$  ensures that the electromagnetic modes can be classified as either TE-like or TM-like, which are decoupled from each other [48]. The TE (TM) modes are distinguished by having a nonvanishing  $H_z$  ( $E_z$ ) field component at the  $z = h/2$  midplane, as shown in Fig. 3(d).

In what follows, the TE (TM) nature of the modes will be used to emulate the  $\uparrow$  ( $\downarrow$ ) isospin components, while the midplane symmetry breaking ( $\Delta g \equiv |g_{\text{top}} - g_{\text{bot}}| \neq 0$ ) will be used to emulate the SOC [34,35]. We use the frequency ordering of the  $\mathbf{p} = (\mathbf{p}_x, \mathbf{p}_y)$  and  $\mathbf{d} = (\mathbf{d}_{xy}, \mathbf{d}_{x^2-y^2})$  orbitals with respect to the photonic band gap at the  $\Gamma$  point to classify the structures as trivial or topological [21,38,40].

Using COMSOL simulations, we designed the unit cells shown in Fig. 3(a) for two types of PhCs satisfying the following criteria for the TE (TM) modes: (i) frequency-degeneracy at the  $\Gamma$  point for both PhCs, (ii) inverted photonic band structures (topological for one mode, trivial for the other) for a PHOTI-type PhC shown in Fig. 3(b), and (iii) similar photonic band structures (topological or trivial for both modes) for the other type of a PhC. A PHOTI corresponding to (ii)—trivial TE mode and a topological TM mode—is shown in Fig. 3(b), while a spin-PHOTI corresponding to (iii)—topological for both modes—is shown in Fig. 3(c). Both structures have symmetric air gaps, and the midplane orbital profiles of the TE ( $H_z$ ) and TM ( $E_z$ ) modes corresponding to the four bands below the band gap are shown in Fig. 3(d), where the left (right) column corresponds to a PHOTI (spin-PHOTI) structure.

To demonstrate that the designed PHOTI and spin-PHOTI structures emulate the corresponding phases described by the TB model given by Eq. (1), we provide a mapping of the photonic model to the TB model in the Supplemental Material [45] relying on the spatial symmetries of the PhC and chiral symmetry [49], as well as investigating phase transitions produced by the SOC-emulating air-gap asymmetry  $\Delta g \neq 0$  by comparing the band structures calculated from the TB model shown in Figs. 4(a) and 4(b) to the first-principles photonic band structures shown in Figs. 4(c) and 4(d). No photonic band gap closing occurs in the case of the PHOTI [Fig. 4(d)]. On the other hand, complete band gap closing for  $\Delta g = \Delta g^{(\text{th})}$  is observed for the spin-PHOTI system, as indicated in Fig. 4(c). Further increase in the effective SOC term ( $\Delta g > \Delta g^{(\text{th})}$ ) reopens the band gap [10] and induces a phase transition from the spin-PHOTI to PHOTI phase (see Supplemental Material [45]).

Next, we demonstrate that interfacing a photonic structure possessing quantized bulk invariants with a trivial PhC produces corner states with correct multiplicities predicted

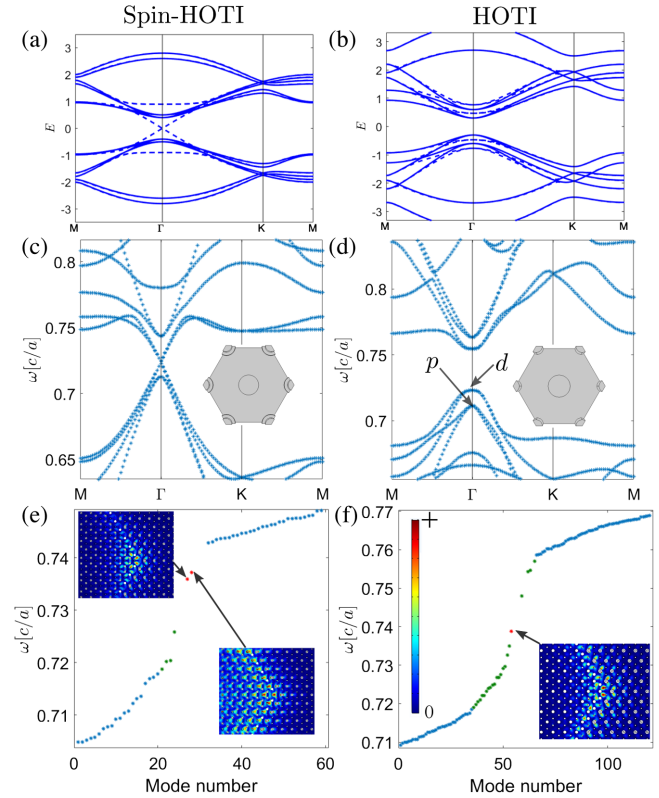


FIG. 4. Comparison between HOTIs based on the TB model and their photonic counterparts: bulk bands (a)–(d) and corner states (e)–(f). Left column: spin-HOTI (a) and spin-PHOTI (c) phases. Right column: HOTI (b) and PHOTI (d) phases. (a) Spin-HOTI bands without (with) the SOC term: solid (dashed:  $\lambda_{\text{SOC}} = \lambda_{\text{SOC}}^{\text{th}}$ ) lines. (b) Same as (a), but for HOTIs. (c) Photonic band structure for a spin-PHOTI phase with  $\Delta g = \Delta g^{(\text{th})}$ . Inset: top view of the unit cell. (d) Same as (c), but for a PHOTI phase.  $p, d$  orbitals are marked with arrows. (e) Photonic corner energy spectrum of a spin-PHOTI and (f) HOTI interfacing a trivial phase at  $120^\circ$  corner. Insets:  $|\mathbf{E}|^2$  [top of (e) and bottom of (f)] and  $|\mathbf{H}|^2$  [bottom of (e)] profiles of the corner modes. Parameters: Table S2 [45].

by the TB model of spinful HOTIs. For the PHOTI shown in Fig. 3(c), we indeed find a single corner state marked by an arrow in Fig. 4(f) and plotted at a  $120^\circ$  corner in the inset. We used edge roughening [21] to increase the edge band gap size (see Supplemental Material [45]).

Photonic analog of the degenerate ZCS pairs predicted by the TB model is constructed by interfacing a trivial PhC with a spin-PHOTI that was chosen to have the same parameters as the structure shown in Fig. 3(c), but a smaller air-gap asymmetry  $\Delta g < \Delta g^{(\text{th})}$ . Indeed, two nearly degenerate corner states marked with arrows in Fig. 4(e) were found. Field intensities  $|\mathbf{E}|^2$  and  $|\mathbf{H}|^2$  of the two corner states plotted in the inset show distinct spatial profiles and polarizations, which is equivalent to having spin texture. The ratio of the average values at the mid-plane of  $E_z$  and  $H_z \sqrt{\mu_0/\epsilon_0}$  determines the pseudospin texture of the ZCSs,

where  $\mu_0$  and  $\epsilon_0$  are the free space permeability and permittivity, respectively.

Several differences between the predictions of the simplified TB model and the results of the continuum electromagnetic calculation are notable. The edge modes shown in Fig. 4(e) and (f) as green dots appear only in the lower half of the bulk photonic band gap (compare with Fig. 2(a),(b)) due to slight mismatch of the band gaps between the trivial and PHOTI phases. This mismatch is also responsible for the spectral shift of the corner state away from the mid-gap frequency and the lack of exact degeneracy between the corner states.

In summary, we have investigated higher-order topological insulating phases on a hexagonal lattice with spin-dependent Kekulé textures. When spin-flipping perturbations, such as spin-orbit coupling, are included in a tight-binding model, two types of insulating topological phases are predicted: a spin-HOTI possessing two independent fractionally quantized bulk invariants  $Q_c^{\uparrow\downarrow}$ , and a HOTI possessing just one such invariant  $Q_c = Q_c^{\uparrow} + Q_c^{\downarrow}$ . A bulk-boundary correspondence between such bulk invariants and the existence of corner states is established, and their photonic analogs are proposed. Our results present an opportunity for future development of novel photonic devices with active switching of their topological corner states by controlling the midplane mirror symmetry, thereby inducing a topological phase transition. Condensed matter realization of the spin-HOTI phase with  $\Delta_{\uparrow} = \Delta_{\downarrow}$  is possible using a platform such as CO molecules deposited on Cu [18]. An effective SOC can be introduced by applying a magnetic field, which would introduce a phase transition to a quantum Hall phase instead of a QSH phase.

This work was supported by the Office of Naval Research Grant No. N00014-21-1-2056, National Science Foundation Grant No. NNCI-1542081, and the Army Research Office Grant W911NF2110180. M. J. also acknowledges the support from the Kwanjeong Fellowship from the Kwanjeong Educational Foundation.

\*rag298@cornell.edu

- [1] C. L. Kane and E. J. Mele, *Phys. Rev. Lett.* **95**, 226801 (2005).
- [2] B. A. Bernevig and S.-C. Zhang, *Phys. Rev. Lett.* **96**, 106802 (2006).
- [3] T. Jungwirth, J. Wunderlich, and K. Olejník, *Nat. Mater.* **11**, 382 (2012).
- [4] T. Kimura, Y. Otani, T. Sato, S. Takahashi, and S. Maekawa, *Phys. Rev. Lett.* **98**, 156601 (2007).
- [5] X.-L. Qi, Y.-S. Wu, and S.-C. Zhang, *Phys. Rev. B* **74**, 085308 (2006).
- [6] F. D. M. Haldane, *Phys. Rev. Lett.* **61**, 2015 (1988).
- [7] B. A. Bernevig, T. L. Hughes, and S.-C. Zhang, *Science* **314**, 1757 (2006).
- [8] N. H. D. Khang, Y. Ueda, and P. N. Hai, *Nat. Mater.* **17**, 808 (2018).
- [9] M. Jamali, J. S. Lee, J. S. Jeong, F. Mahfouzi, Y. Lv, Z. Zhao, B. K. Nikolić, K. A. Mkhoyan, N. Samarth, and J.-P. Wang, *Nano Lett.* **15**, 7126 (2015).
- [10] J. K. Asbóth, L. Oroszlány, and A. Pályi, *Lect. Notes Phys.* **919**, 997 (2016).
- [11] A. Kitaev, *AIP Conf. Proc.* **1134**, 22 (2009).
- [12] W. A. Benalcazar, B. A. Bernevig, and T. L. Hughes, *Science* **357**, 61 (2017).
- [13] F. Schindler, A. M. Cook, M. G. Vergniory, Z. Wang, S. S. Parkin, B. A. Bernevig, and T. Neupert, *Sci. Adv.* **4**, eaat0346 (2018).
- [14] C. W. Peterson, W. A. Benalcazar, T. L. Hughes, and G. Bahl, *Nature (London)* **555**, 346 (2018).
- [15] S. Franca, J. van den Brink, and I. Fulga, *Phys. Rev. B* **98**, 201114(R) (2018).
- [16] F. Schindler, M. Brzezińska, W. A. Benalcazar, M. Iraola, A. Bouhon, S. S. Tsirkin, M. G. Vergniory, and T. Neupert, *Phys. Rev. Research* **1**, 033074 (2019).
- [17] S. Kooi, G. van Miert, and C. Ortix, *Quantum Mater.* **6**, 1 (2021).
- [18] S. E. Freeney, J. J. Van den Broeke, A. J. J. Harsveld van der Veen, I. Swart, and C. Morai Smith, *Phys. Rev. Lett.* **124**, 236404 (2020).
- [19] S. Kempkes, M. Slot, J. van Den Broeke, P. Capiod, W. Benalcazar, D. Vanmaekelbergh, D. Bercioux, I. Swart, and C. M. Smith, *Nat. Mater.* **18**, 1292 (2019).
- [20] B.-Y. Xie, H.-F. Wang, H.-X. Wang, X.-Y. Zhu, J.-H. Jiang, M.-H. Lu, and Y.-F. Chen, *Phys. Rev. B* **98**, 205147 (2018).
- [21] M. Jung, R. G. Gladstone, and G. B. Shvets, *Adv. Opt. Photonics* **2**, 046003 (2020).
- [22] B.-Y. Xie, G.-X. Su, H.-F. Wang, H. Su, X.-P. Shen, P. Zhan, M.-H. Lu, Z.-L. Wang, and Y.-F. Chen, *Phys. Rev. Lett.* **122**, 233903 (2019).
- [23] X.-D. Chen, W.-M. Deng, F.-L. Shi, F.-L. Zhao, M. Chen, and J.-W. Dong, *Phys. Rev. Lett.* **122**, 233902 (2019).
- [24] Y. Chen, F. Meng, Z. Lan, B. Jia, and X. Huang, *Phys. Rev. Applied* **15**, 034053 (2021).
- [25] J. Noh, W. A. Benalcazar, S. Huang, M. J. Collins, K. P. Chen, T. L. Hughes, and M. C. Rechtsman, *Nat. Photonics* **12**, 408 (2018).
- [26] B. Xie, G. Su, H.-F. Wang, F. Liu, L. Hu, S.-Y. Yu, P. Zhan, M.-H. Lu, Z. Wang, and Y.-F. Chen, *Nat. Commun.* **11**, 1 (2020).
- [27] Y. Ota, F. Liu, R. Katsumi, K. Watanabe, K. Wakabayashi, Y. Arakawa, and S. Iwamoto, *Optica* **6**, 786 (2019).
- [28] C. W. Peterson, T. Li, W. A. Benalcazar, T. L. Hughes, and G. Bahl, *Science* **368**, 1114 (2020).
- [29] L. J. Maczewsky, B. Höckendorf, M. Kremer, T. Biesenthal, M. Heinrich, A. Alvermann, H. Fehske, and A. Szameit, *Nat. Mater.* **19**, 855 (2020).
- [30] Z. Qiao, W.-K. Tse, H. Jiang, Y. Yao, and Q. Niu, *Phys. Rev. Lett.* **107**, 256801 (2011).
- [31] M. J. Park, Y. Kim, G. Y. Cho, and S. B. Lee, *Phys. Rev. Lett.* **123**, 216803 (2019).
- [32] D. Pesin and A. H. MacDonald, *Nat. Mater.* **11**, 409 (2012).
- [33] J. Lu, C. Qiu, W. Deng, X. Huang, F. Li, F. Zhang, S. Chen, and Z. Liu, *Phys. Rev. Lett.* **120**, 116802 (2018).

- [34] T. Ma, A. B. Khanikaev, S. H. Mousavi, and G. Shvets, *Phys. Rev. Lett.* **114**, 127401 (2015).
- [35] T. Ma and G. Shvets, *Phys. Rev. B* **95**, 165102 (2017).
- [36] R. G. Gladstone, M. Jung, Y. Han, and G. Shvets, *Phys. Rev. B* **100**, 245417 (2019).
- [37] M. Farjam and H. Rafii-Tabar, *Phys. Rev. B* **79**, 045417 (2009).
- [38] L.-H. Wu and X. Hu, *Sci. Rep.* **6**, 24347 (2016).
- [39] W. A. Benalcazar, T. Li, and T. L. Hughes, *Phys. Rev. B* **99**, 245151 (2019).
- [40] L.-H. Wu and X. Hu, *Phys. Rev. Lett.* **114**, 223901 (2015).
- [41] Z.-Z. Yang, X. Li, Y.-Y. Peng, X.-Y. Zou, and J.-C. Cheng, *Phys. Rev. Lett.* **125**, 255502 (2020).
- [42] S. S. Kruk, W. Gao, D.-Y. Choi, T. Zentgraf, S. Zhang, and Y. Kivshar, *Nano Lett.* **21**, 4592 (2021).
- [43] N. W. Ashcroft *et al.*, *Solid State Physics* (Holt, Rinehart and Winston, New York, London, 1976).
- [44] M. S. Dresselhaus, G. Dresselhaus, and A. Jorio, *Group Theory: Application to the Physics of Condensed Matter* (Springer Science & Business Media, New York, 2007).
- [45] See Supplemental Material at <http://link.aps.org/supplemental/10.1103/PhysRevLett.128.026801> for analytic calculations, additional phase diagrams and simulation results, discussion of localized density of states and bulk-boundary correspondence and parameters for the designs used in the manuscript.
- [46] L. J. Maczewsky, B. Höckendorf, M. Kremer, T. Biesenthal, M. Heinrich, A. Alvermann, H. Fehske, and A. Szameit, *Nat. Mater.* **19**, 855 (2020).
- [47] C.-Y. Hou, C. Chamon, and C. Mudry, *Phys. Rev. Lett.* **98**, 186809 (2007).
- [48] J. D. Joannopoulos, S. G. Johnson, J. N. Winn, and R. D. Meade, *Molding the Flow of Light* (Princeton University Press, Princeton, NJ, 2008).
- [49] Z. Xiong, W. Chen, P. Wang, and Y. Chen, *Opt. Express* **25**, 29822 (2017).